Magn Reson Med Sci 2018; 17; 58–66
doi:10.2463/mrms.mp.2017-0035
Published Online: September 4, 2017

MAJOR PAPER

In vitro Study of Serial Changes to Carmustine Wafers (Gliadel) with MR Imaging and Computed Tomography

Satoshi Doishita[1*], Taro Shimono[1], Tetsuya Yoneda[2], Eiji Yamada[3], Taro Tsukamoto[1], Daichi Takemori[3], Daisuke Kimura[3], Hiroyuki Tatekawa[1], Shinichi Sakamoto[1], and Yukio Miki[1]

Purpose: Implantation of carmustine wafers (Gliadel) *in vivo* is accompanied by characteristic serial changes on MRI and CT, such as transient hyperintensity of the wafers on T_1-weighted images (T_1WIs) and considerable gas accumulation in surgical resection cavities. The purpose of this study was to evaluate intrinsic imaging changes to carmustine wafers *in vitro*.

Methods: Three phantoms simulating a surgical resection cavity were constructed. Each contained either a carmustine wafer fixed with oxidized regenerated cellulose and fibrin sealant, an unfixed carmustine wafer, or a fixed polyethylene control disk, immersed in phosphate-buffered saline. Image acquisition of the phantoms was performed on MRI and CT until 182 days after construction. The radiological appearances of the object in each phantom were assessed by visual evaluation and quantification of the region of interest. The volume of gas around the objects at 24 h after constructing the phantoms was also measured.

Results: The carmustine wafers showed low signal intensities on T_1WIs and T_2-weighted images (T_2WIs), and high densities on CT images at 24 h. The signal intensities and CT densities gradually approximated those of saline over a period of months. However, the carmustine wafers never showed hyperintensity on T_1WIs *in vitro*. The fixed carmustine wafer showed slower radiological changes, as compared to the unfixed wafer. The gas volume around the fixed carmustine wafer was greater than that around the fixed control disk.

Conclusion: Changes to the carmustine wafers probably reflected penetration of fluid inside and degradation of the hydrophobic matrix. Reported transient hyperintensity of wafers on T_1WIs *in vivo* is regarded as the result of biological reactions, whereas the initial production of gas is considered as an intrinsic characteristic of wafers.

Keywords: *carmustine wafer, Gliadel, bis-chloroethylnitrosourea wafer, in vitro, phantom*

Introduction

Local chemotherapy with 1,3-bis-(2-chloroethyl)-1-nitrosourea or carmustine wafer (Gliadel, Eisai Co., Ltd., Tokyo, Japan) implantation after tumor resection is an approved treatment for newly diagnosed or recurrent malignant gliomas in many countries.[1,2] The matrix of the carmustine wafer consists of hydrophobic copolymers with 1,3-bis(p-carboxyphenoxy)propane and sebacic acid in a molar ratio of 20:80 (p[CPP-SA, 20:80]). Gradual hydrolysis of the anhydride bonds in the matrix enables release of the incorporated carmustine in a sustained and controlled manner.[3,4] The combination of local chemotherapy with carmustine wafers directly to the tumor site and more delayed systemic chemotherapy theoretically allows for synergic adjuvant therapy to commence immediately after surgery.[5]

Several reports on serial changes to carmustine wafers *per se*, surgical resection cavity and adjacent brain parenchyma on MRI and CT after implantation in the clinical setting have been published.[6–13] The wafers have been reported to be hypointense on T_1-weighted images (T_1WIs) and T_2-weighted images (T_2WIs) within the first week, show transient hyperintensity on T_1WIs at around 1 or 2 months, and become poorly visible on both sequences at 3 to 12

[1]Department of Diagnostic and Interventional Radiology, Osaka City University Graduate School of Medicine, 1-4-3 Asahi-machi, Abeno-ku, Osaka, Osaka 545-8585, Japan
[2]Department of Medical Physics in Advanced Biomedical Sciences, Faculty of Life Sciences, Kumamoto University, Kumamoto, Japan
[3]Department of Radiological Technology, Osaka City University Hospital, Osaka, Japan
*Corresponding author, Phone: +81-6-6645-3831, Fax: +81-6-6646-6655, E-mail: sd@med.osaka-cu.ac.jp

Received: March 1, 2017 | Accepted: July 5, 2017

months postoperatively.[6,10–12] On CT, the wafers initially appear hyperdense, then gradually decrease visibility, and become poorly visible after 3 months post-implantation in operated patients.[6,12] As for the surgical resection cavity and adjacent brain parenchyma, various changes such as considerable gas and restricted diffusivity around wafers, hyperintense areas at the rim of surgical resection cavity on T_2WIs and surgical bed cysts have been observed.[6,7,9–13]

These changes associated with carmustine wafers on MRI and CT are unique. However, the mechanisms underlying these changes have not yet been clarified.[12] In particular, it remains unclear as to whether the transient hyperintensity of the wafers on T_1WIs and a considerable amount of gas around the wafers represent intrinsic characteristics or are the result of interactions between the wafers and biological reactions because no previous study has investigated the imaging changes associated with carmustine wafers *in vitro*.

The goal of this study was to elucidate the *in vitro* imaging changes to wafers under the condition where the influence of biological reactions was removed.

Materials and Methods

Phantoms and references

Three different phantoms simulating a surgical resection cavity were constructed. Each phantom consisted of a Falcon 50-mL polypropylene conical tube, an acrylic column, a 5-mL styrol bottle, 20 mL of phosphate-buffered saline (PBS; 0.3 mM, pH 7.1), and either a carmustine wafer or a control disk, with or without oxidized regenerated cellulose (Surgicel, Ethicon, Johnson & Johnson, Somerville, NJ, USA) and fibrin sealant (Beriplast P, CSL Behring, King of Prussia, PA, USA) (Fig. 1). A polyethylene disk of the same size as a carmustine wafer (1.4 cm in diameter and 1.3 mm thick) was used as the control. The 5-mL styrol bottle was attached to the cap of the falcon 50-mL polypropylene conical tube of each phantom in order to make the object stay immersed in PBS and inside the MRI scan range even when it floated.

In the clinical setting, carmustine wafers are usually placed with fixing agents and the surgical resection cavity is irrigated with perfusate.[14] Phantom B in the present study thus represented a surgical resection cavity implanted with a carmustine wafer fixed with oxidized regenerated cellulose and fibrin sealant. Phantom A, which contained a polyethylene disk instead of a carmustine wafer, was constructed as a control. On the other hand, phantom C with an unfixed carmustine wafer was designed to investigate the effect of oxidized regenerated cellulose and fibrin sealant on images in comparison with phantom B. PBS of pH 7.1 was chosen for the present study because surgical resection cavities *in vivo* are considered to be under weak acidic conditions. All phantoms were incubated at 37°C. The PBS was changed daily to imitate the excretion of substances out of a surgical resection cavity.

Mixed solutions composed of manganese(II) chloride tetrahydrate with 40 mg/L manganese (Bothdel Oral Solution 10, Kyowa Hakko Kirin, Tokyo, Japan) and physiological saline in a volume ratio of 13:87 were prepared as MRI references substituting for the brain. As a CT reference substituting for the brain, a solution of 8% glucose was prepared.

MRI protocols and analysis

Magnetic resonance image acquisition was performed on a 3-Tesla scanner (Achieva, Philips Medical Systems, Best, The Netherlands) using a 32-channel head coil. Imaging sequences included axial T_1-weighted spin echo (SE) (TR, 400 msec; TE, 13 msec; slice thickness, 3.0 mm; no gap; FOV, 200 × 200 mm^2; matrix, 512 × 333), axial T_2-weighted turbo spin echo (TSE) (TR, 4152 msec; TE, 100 msec; TSE factor, 11; slice thickness, 3.0 mm; no gap; FOV, 200 × 200 mm^2; matrix, 512 × 307), 3D T_1-weighted volume isotropic

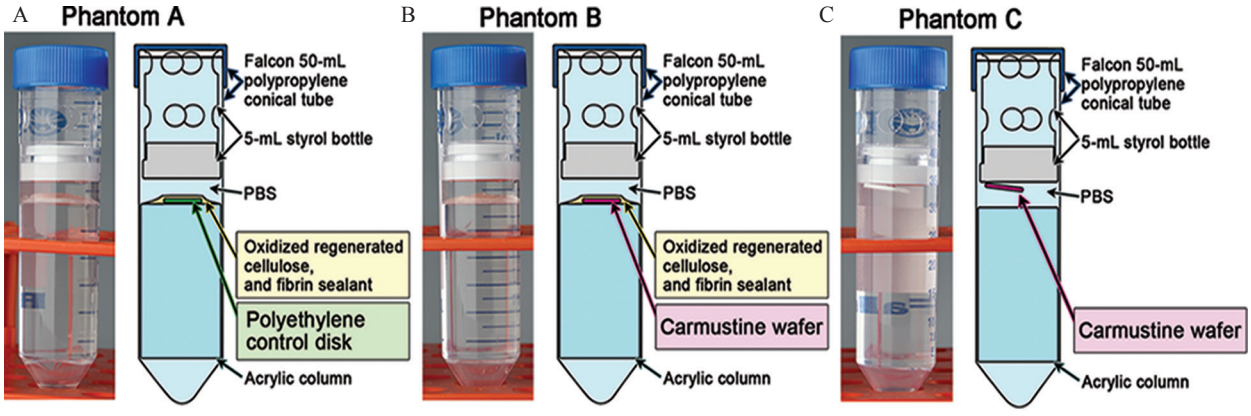

Fig. 1 Photographs and schemas of phantom A (**A**), phantom B (**B**) and phantom C (**C**). Photographs were taken at 2 h after construction of phantoms. Phantom B represented a surgical resection cavity implanted with a carmustine wafer fixed with oxidized regenerated cellulose and fibrin sealant. Phantom A, which contained a polyethylene disk instead of a carmustine wafer, was constructed as a control. Phantom C with an unfixed carmustine wafer was designed to investigate the effect of fixing agents in comparison with phantom B.

TSE acquisition (VISTA) (TR, 330 msec; TE, 20 msec; TSE factor, 9; flip angle, 80°; matrix, 400 × 400 × 45; and voxel size, 0.5 × 0.5 × 0.5 mm^3) and 3D T_2-weighted VISTA (TR, 2000 msec; TE, 120 msec; TSE factor, 40; flip angle, 90°; matrix, 400 × 396 × 45; voxel size, 0.5 × 0.54 × 0.5 mm^3). In addition, a mixed sequence (TR-SE, 920 msec; TR-inversion recovery, 2300 msec; TE 1, 30 msec; TE 2, 60 msec; TE 3, 90 msec; TE 4, 120 msec; inversion time, 500 msec; slice thickness, 10 mm; FOV 250 × 250 mm^2; matrix, 128 × 128) implemented on the MRI scanner was performed to verify that the T_1 and T_2 values of the MRI references were similar to the reported values of the brain at 3 Tesla (white matter, T_1: 1084 ± 45 msec, T_2: 69 ± 3 msec; gray matter, T_1: 1820 ± 114 msec, T_2: 99 ± 7 msec).[15,16]

Magnetic resonance images of all of the phantoms were acquired sequentially at 24 h (just before the first exchange of saline), and at 14, 28, 42, 70, 98, 126, 154 and 182 days following placement. The three phantoms and the two MRI references were placed in an axial plane and kept still for 15 min before acquiring images to suppress the motion of the liquid. The T_1 and T_2 values of the MRI references at every acquisition time were calculated as the average values of two 15 × 10 mm^2 rectangular ROIs placed on the MRI references on T_1 and T_2 maps (mixed sequence), respectively.

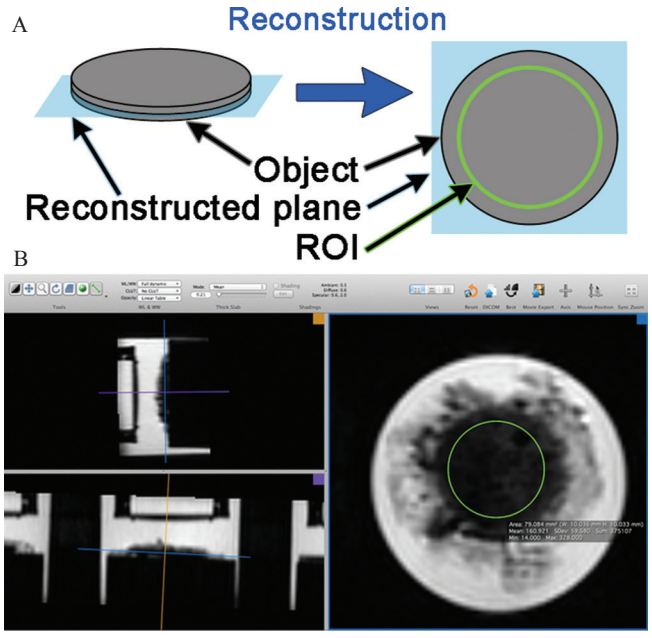

Fig. 2 Method (**A**) and a screen capture sample (**B**) of ROI placement. First, the plane passing through the center of and parallel to the base of each object was reconstructed with 3D T_1-weighted volume isotropic turbo spin echo acquisition (VISTA), 3D T_2-weighted VISTA, and thin-slice CT images. Next, a 10 mm-diameter circular ROI was manually placed on the center of each object on the reconstructed plane. If an object collapsed, only the largest fragment was subject to evaluation. If a placed object or its largest fragment became smaller than 10 mm, a maximal elliptical ROI was placed instead. DICOM viewer OsiriX (Pixmeo SARL, Bernex, Switzerland) was used for placing ROI (**B**).

Two methods were adopted for the assessment of the MRI appearance of the carmustine wafers themselves.

The first was a qualitative analysis based on visual evaluation. Two observers (T.T. and S.D., with 6 and 7 years of experience in radiology, respectively) separately graded the degree of visualization of the placed objects on T_1-weighted SE and T_2-weighted TSE images. If an object collapsed, only the largest fragment was subject to evaluation. Each observer individually reviewed the images and discordance between the observers was subject to re-review to achieve consensus. The predominant signal intensities of the placed objects were graded as follows: a 1–5 ordinal scale for T_1WIs (1, lower than saline; 2, isointense to saline or difficult to detect; 3, between saline and the MRI references substituting for the brain; 4, isointense to the MRI references; and 5, higher than the MRI references) and a 1–4 ordinal scale for T_2WIs (1, lower than the MRI references substituting for the brain; 2, isointense to the MRI references; 3, between the MRI references and saline; and 4, isointense to saline or difficult to detect).

The second evaluation was a quantitative analysis using ROIs (Fig. 2). DICOM viewer OsiriX (v5.8.5 32-bit, Pixmeo SARL, Bernex, Switzerland) was used for placing ROIs. The plane passing through the center of and parallel to the base of each object was reconstructed with 3D T_1-weighted VISTA and 3D T_2-weighted VISTA images. A 10 mm-diameter circular ROI was then manually placed on the center of each object by the two observers in consensus. Each ROI placement was conducted once. If an object collapsed, only the largest fragment was subject to evaluation. If a placed object or its largest fragment became smaller than 10 mm, a maximal elliptical ROI was placed instead. Care was taken to avoid contamination of the signal from saline. Because MRI signal intensity is not a comparable value, the average signal intensities of the same rectangular ROIs as those on T_1 and T_2 maps were calculated using 3D T_1-weighted VISTA and 3D T_2-weighted VISTA images and the signal ratios of the ROIs of the placed objects to those of the references were evaluated thereafter.

CT protocols and analysis

CT image acquisition was performed on a 64-slice CT scanner (Somatom, Siemens Healthcare, Erlangen, Germany) with non-helical scans. The parameters of the CT scans included slice thickness, 0.6 mm; FOV, 200 × 200 mm^2; matrix, 512 × 512; tube voltage, 120 kV; tube current, 400 mA. Thick-slice (6-mm slice thickness) and thin-slice (0.6-mm slice thickness) axial images were reconstructed.

The imaging schedule of CT was as follows. First, the CT reference substituting for the brain was prepared and the density of a 15 × 10 mm^2 rectangular ROI on a thick-slice CT image was measured. Then, CT images of the unfixed carmustine wafer in phantom C were obtained at 1.5 h after placement into saline to clarify the original CT value of carmustine wafer. Subsequently, images of all of the phantoms were acquired sequentially at 24 h (just before the first

exchange of saline), and at 14, 28, 42, 70, 98, 126, 154 and 182 days following placement.

Two methods, qualitative analysis based on visual evaluation and quantitative ROI analysis, were adopted for the assessment of the CT appearance of the carmustine wafers similarly as in MRI analysis. In qualitative analysis, thick-slice CT images were evaluated and the predominant densities of the placed objects were graded using a 1–5 ordinal scale (1, lower than saline; 2, isodense to saline or difficult to detect; 3, between saline and the CT reference substituting for the brain; 4, isodense to the CT reference; and 5, higher than the CT reference). In quantitative analysis, thin-slice CT images were used and CT values of the ROIs of the objects themselves were evaluated.

Whether the carmustine wafer of phantom C was floating (beneath the styrol bottle) or sunk (on the acrylic column) was also recorded at every CT image acquisition time because it was not fixed with oxidized regenerated cellulose and fibrin sealant.

To assess the initial production of gas, the volume of the gas within a distance of 3 mm from the surface of the control disk in phantom A and the carmustine wafer in phantom B was calculated with ImageJ software (version 1.51g, National Institutes of Health, Bethesda, MD, USA) using thin-slice CT images obtained at 24 h after placement (Fig. 3).

Statistics

Interobserver agreement for MRI signal intensities and CT density was assessed by calculating Cohen's weighted kappa (κ) coefficients in qualitative analysis. The strength of agreement was considered as follows: κ values of 0.00–0.20, slight; 0.21–0.40, fair; 0.41–0.60, moderate; 0.61–0.80, substantial; and 0.81–1.00, almost perfect.[17] R (version 3.2.3, R Foundation for Statistical Computing, Vienna, Austria) was used for statistical analysis.

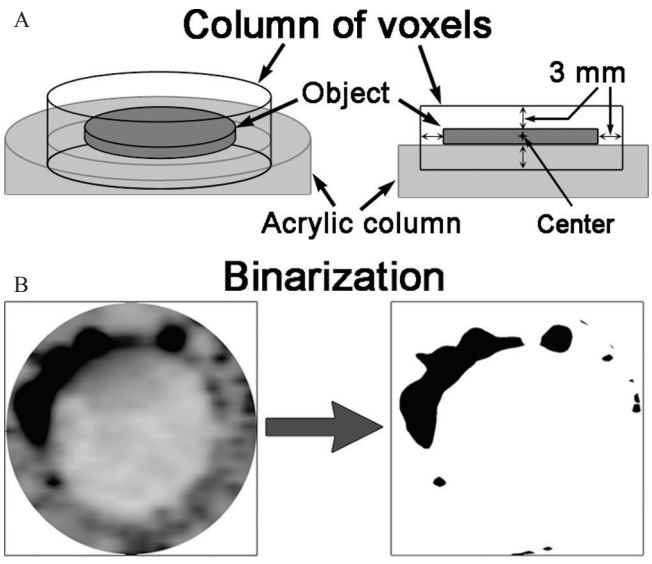

Fig. 3 Method for measurement of gas volume. First, planes passing through the center of and parallel to the base of the object were reconstructed with thin-slice CT images at 24 h after placement (just before the first exchange of saline), using DICOM viewer OsiriX (Pixmeo SARL, Bernex, Switzerland). Next, voxels within the column 3 mm larger in each direction than the placed object were extracted (**A**) and then binarized with threshold of –100 Hounsfield units (HU) using ImageJ software (National Institutes of Health, Bethesda, MD, USA) (**B**). Finally, volume of voxels under the threshold was calculated.

Results

Phantoms over 6 months

The experiment spanned 6 months, and hence two minor damages within the assumption range occurred on phantoms. First, the fixing agents in phantom A peeled off at the last two time points of image acquisition. The assessment of the object itself was possible although it floated. Second, the object collapsed into several fragments in phantom C at the last two time points. The largest fragment of the collapsed object was analyzed.

Serial changes to the carmustine wafers over 6 months on MRI

The T_1 and T_2 values of the MRI references at all nine time points of magnetic resonance image acquisition over a 6-month period were 1114 ± 13 msec (mean ± standard deviation) and 97 ± 1 msec, respectively. The T_1 values were similar to the white matter and T_2 values to the gray matter.

T_1-weighted SE images and T_2-weighted TSE images of all phantoms and MRI references obtained between 24 h to 182 days after construction, which were used for visual evaluation, are displayed in Figs. 4 and 5, respectively. In addition, the time courses regarding the MRI appearance of the carmustine wafers and the polyethylene control disk in both visual evaluation and quantitative ROI analysis are shown in Fig. 6A and B.

In visual evaluation, the polyethylene control disk was graded as lower than saline on T_1WIs and as lower than the MRI references on T_2WIs throughout the whole period. The carmustine wafers were graded similarly to the control disk on both sequences at 24 h after placement. On T_1WIs, both of the carmustine wafers became isointense to saline or difficult to detect during the observation period, with an earlier change in the unfixed carmustine wafer (phantom C). Thus, the carmustine wafers did not appear isointense or hyperintense relative to the MRI references substituting for the brain on T_1WIs throughout the period (Figs. 4 and 6A). On T_2WIs, the intensity of the unfixed carmustine wafer (phantom C) alone became isointense to the MRI references during the period (Figs. 5 and 6B). Interobserver agreement on the grading of T_1WIs was almost perfect (κ = 1.00) and substantial for T_2WIs (κ = 0.78).

In quantitative ROI analysis, the signal ratios of the polyethylene control disk in phantom A to the MRI references remained less than 0.1 on T_1WIs and less than 0.2 on T_2WIs throughout the whole period. The carmustine wafers in phantoms B and C also showed low signal ratios similar to those of the polyethylene disk on both T_1WIs and T_2WIs,

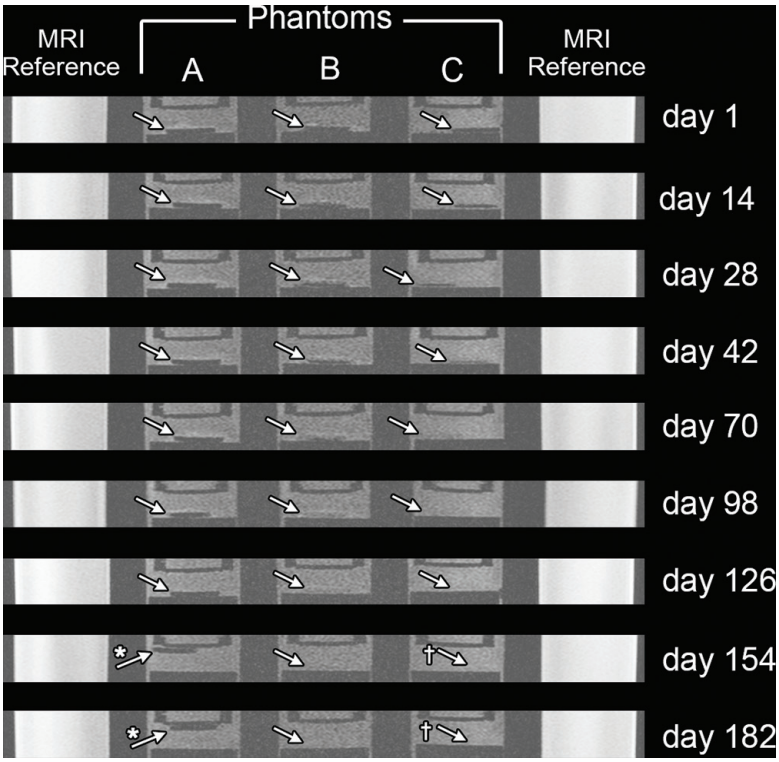

Fig. 4 T_1-weighted spin echo (SE) images of all phantoms and MRI references obtained between 24 h to 182 days after construction. An arrow indicates an object (a carmustine wafer or a control disk). An asterisk (*) indicates that the placed object was floating because of peeling off of the fixing agents. A dagger (†) indicates that the largest fragment of the collapsed object was analyzed. The carmustine wafers in phantoms B and C did not show transient hyperintensity *in vitro*.

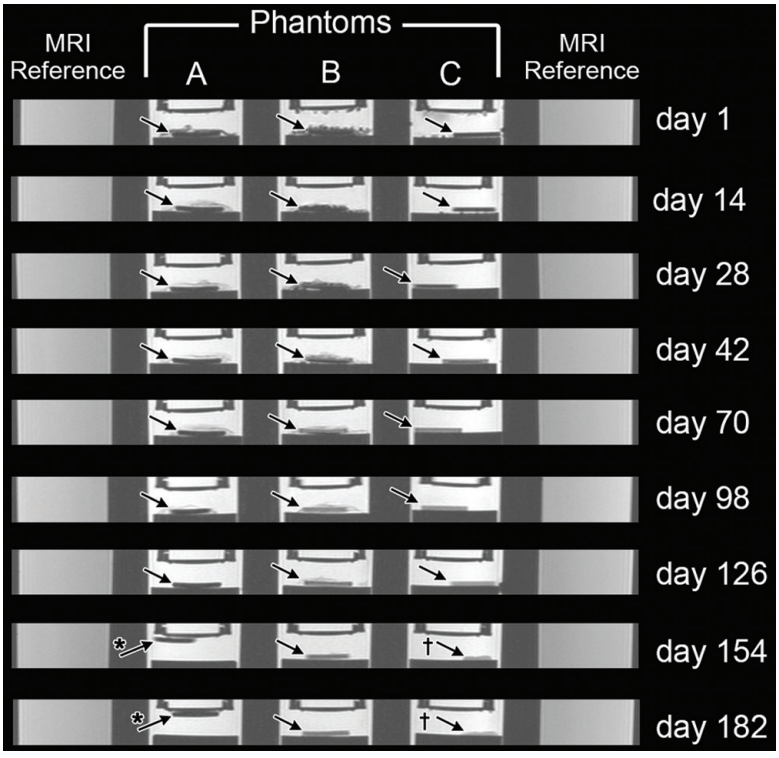

Fig. 5 T_2-weighted turbo spin echo (TSE) images of all phantoms and MRI references obtained between 24 h to 182 days after construction. An arrow indicates an object (a carmustine wafer or a control disk). An asterisk (*) indicates that the placed object was floating because of peeling off of the fixing agents. A dagger (†) indicates that the largest fragment of the collapsed object was analyzed.

initially at 24 h after placement. However, the signal ratios of the carmustine wafers to the references then gradually increased on both sequences over a period of months (Fig. 6A and B). Nevertheless, the signal ratios of the carmustine wafers to the MRI references substituting for the brain did not exceed 1.0 on T_1WIs (Fig. 6A). The carmustine wafer fixed with oxidized regenerated cellulose and fibrin sealant (phantom B) showed a slower increase in the signal ratios on both sequences, as compared to the unfixed wafer (phantom C).

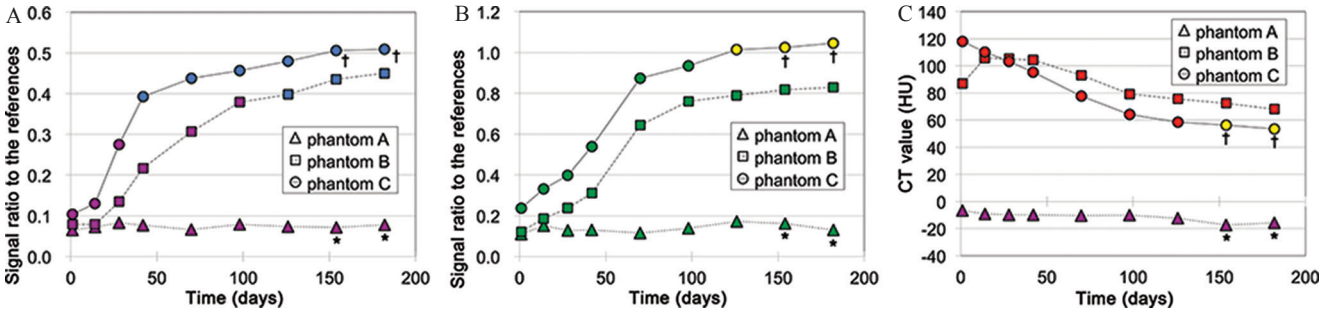

Fig. 6 The results of visual evaluation and quantitative ROI analysis of the appearances of the placed objects on T_1-weighted images (T_1WIs) (**A**), T_2-weighted images (T_2WIs) (**B**), and CT images (**C**) from 24 h to 182 days after construction of the phantoms. The value of each data point (MRI signal ratio or CT value) represents the result of quantitative ROI analysis. The lines in each graph are not exact fits to the data, but simply connect the data points. The color of each data point is the result of visual evaluation as follows: purple, lower than saline; blue, isointense/isodense to saline or difficult to detect; green, lower than the reference(s); yellow, isointense/isodense to the reference(s); and red, higher than the reference(s). An asterisk (*) indicates that the placed object was floating because of peeling off of the fixing agents. A dagger (†) indicates that the largest fragment of the collapsed object was analyzed. HU, Hounsfield units.

Serial changes to the carmustine wafers over 6 months on CT

Prepared 8% glucose solution showed 36 Hounsfield units (HU) and therefore considered suitable for a CT reference substituting for the brain in visual evaluation (Fig. 7A).

At 1.5 h after placement into PBS, the unfixed carmustine wafer in phantom C was graded as lower than saline in visual evaluation (Fig. 7B). In quantitative ROI analysis, the CT value of the wafer was −39.1 HU at that time.

Thick-slice CT images of all phantoms obtained between 24 h and 182 days after construction, which were used for visual evaluation, are shown in Fig. 7C. In addition, Fig. 6C graphically demonstrates the time course of the CT appearance of the carmustine wafers and the polyethylene control disk in both visual evaluation and quantitative ROI analysis during the same period.

In visual evaluation of CT densities, the polyethylene control disk remained lower than saline at all times. In contrast, the carmustine wafers were graded as higher than the CT reference substituting for the brain at 24 h after placement into saline and afterwards. Only the density of the unfixed carmustine wafer (phantom C) changed to isodense to the CT reference during the observation period (Figs. 6C and 7C). Interobserver agreement on the grading of CT images was almost perfect ($\kappa = 0.846$).

In quantitative ROI analysis, the CT value of the polyethylene control disk was less than 0 HU throughout the whole period. On the other hand, the CT values of the carmustine wafers in phantoms B and C were both greater than 80 HU at 24 h after placement. Subsequently, the CT values of the carmustine wafers tended to decrease gradually over a time period of months (Fig. 6C). Change in the fixed carmustine wafer (phantom B) was slower than in the unfixed wafer (phantom C) also on CT.

The unfixed wafer in phantom C was floating in saline at 1.5 h after placement (Fig. 7B), turned sunk at 24 h after placement and remained so throughout the following 6 months (Fig. 7C).

Initial amount of gas around the carmustine wafers

The gas volume around the fixed carmustine wafer (phantom B) was greater than that around the fixed polyethylene disk (phantom A) at 24 h after placement into saline (Fig. 7D). The measured gas volume and its proportion to the volume of the object in each phantom were as follows: phantom A, 7.7 mm^3, 3.3%; and phantom B, 92.5 mm^3, 46.2%.

Discussion

In the present *in vitro* study, the MRI signal intensities and CT densities of the carmustine wafers gradually approached those of saline over a period of months, with slower changes in the fixed wafer; the carmustine wafers did not show hyperintensity on T_1WIs *in vitro*. In addition, more gas was observed around the fixed carmustine wafer than around the fixed control disk.

Serial changes in imaging appearance of carmustine wafers over a period of months

To date, several studies have reported on the imaging appearance of carmustine wafers themselves *in vivo*. Brem et al. demonstrated that carmustine-loaded p(CPP-SA, 20:80) wafers appeared as bright white lines on CT within 1 to 2 days postoperatively and up to 49 days after surgery in some patients.[18] Thereafter, Prager et al. and Hammoud et al. revealed serial changes in the MRI and CT appearance of carmustine-loaded and empty p(CPP-SA, 20:80) wafers in patients after surgery, with reporting that the presence of carmustine did not affect imaging appearance.[6,7] Prager et al. also reported a transient increase in signal intensity of the wafers on T_1WIs at about 2 months after implantation.[6] Subsequently, Colen et al., Ulmer et al., and Ohue et al.

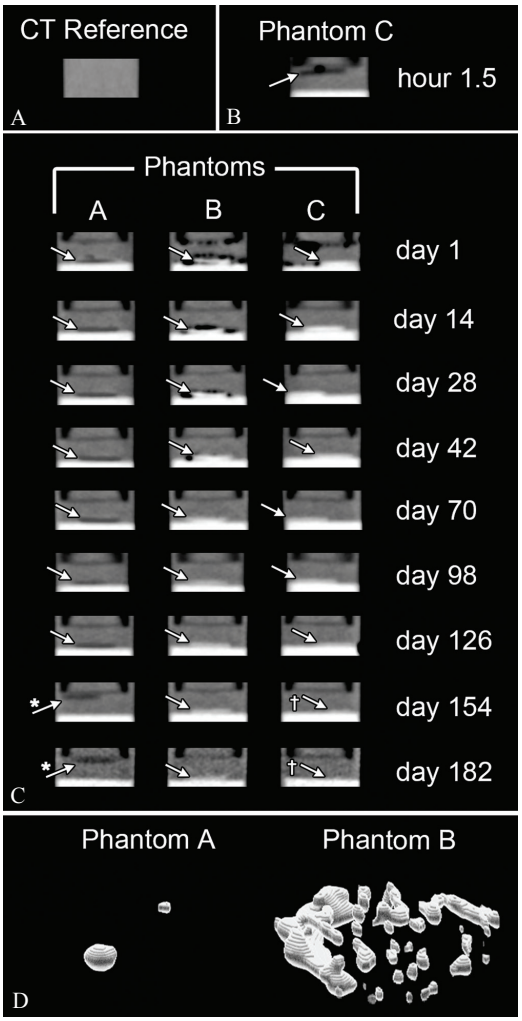

Fig. 7 Thick-slice CT images of the CT reference (**A**), phantom C obtained at 1.5 h after construction (**B**) and all phantoms obtained between 24 h to 182 days after construction (**C**). An arrow indicates an object (a carmustine wafer or a control disk). An asterisk (*) indicates that the placed object was floating because of peeling off of the fixing agents. A dagger (†) indicates that the largest fragment of the collapsed object was analyzed. The window width is set at 200 Hounsfield units (HU) and the window level is set at 40 HU. Volume rendering images of gas within a distance of 3 mm from the surfaces of the placed objects in phantoms A and B at 24 h after construction (**D**), processed with ImageJ software (National Institutes of Health, Bethesda, MD, USA).

demonstrated serial imaging changes to the wafers in patients treated with Gliadel.[10–12] The results of these studies were basically similar as follows. On MRI, the carmustine wafers showed hypointensity on T_1WIs and T_2WIs within the first week, turned hyperintense on T_1WIs at around 1 or 2 months, and appeared poorly visible on both sequences after 3 to 12 months. On CT images, the wafers were initially hyperdense, then gradually decreased visibility and became poorly visible after 3 months.

The findings of this experiment clarified the *in vitro* serial changes to carmustine wafers on MRI and CT. In this study, the MRI intensities and CT densities of the carmustine wafers gradually approached those of saline over a period of months. According to FDA's Docket Management, wafer remnants contained more than 74% of water in weight in two cases of re-operation at 64 and 92 days after implantation.[14] Gradual approach of wafers to saline in terms of MRI intensity and CT density is therefore considered to reflect penetration of fluid inside the wafers, degradation of the hydrophobic matrix and washout of its components.

Unlike previous reports concerning serial radiological changes *in vivo*, the carmustine wafers showed no transient hyperintensity on T_1WIs *in vitro*. Therefore, the hyperintensity on T_1WIs in the clinical setting is probably neither an intrinsic feature of the carmustine wafers nor a result of the interaction between the wafers and fixing agents, but rather probably attributable to the biological reactions to the wafers. Immunoglobulins G, A and M, and glial fibrillary acidic protein were reported to be detected inside the removed remnants of carmustine wafers in a case *in vivo*.[19] In addition, according to the observation using scanning electron microscopy, the porosity of the wafers gradually increased throughout the whole wafer during degradation.[20] Furthermore, other previous studies reported that patients implanted with carmustine wafers had persistent disks *in situ* at the time of autopsy or reoperation up to 68 weeks after implantation.[18,21] Proteinaceous and blood-derived materials deposited inside the porous water-rich remnants may be convincing sources of the hyperintensity on T_1WIs *in vivo*.

Effect of fixing agents on radiological appearance

The carmustine wafer fixed with oxidized regenerated cellulose and fibrin sealant showed slower serial imaging changes, as compared to the unfixed wafer on all images in this study. Oxidized regenerated cellulose is known to significantly decrease the pH of various fluids and degradation of the matrix of biodegradable wafers has been reported to be slower at a lower pH.[3,22] A locally lower pH beyond buffer capacity caused by the oxidized regenerated cellulose is assumed to lead to slower changes in imaging appearance. In addition, gas trapped beneath the fixing agents may have also delayed hydrolysis of the matrix by partially preventing contact of the wafer with the surrounding fluid. Fixation with oxidized regenerated cellulose is a frequently used procedure in the implantation of the carmustine wafers. However, this procedure may slow the rate of hydrolysis of the matrix and probably the release of incorporated carmustine as well, as reflected in visibility on MRI and CT.

Initial gas around carmustine wafers

It is known that a considerable amount of gas is observed in the surgical resection cavities implanted with carmustine wafers, although the source of gas has not yet been identified.[12] Hammoud et al. were the first to measure gas volume in wafer-implanted resection cavities using radiological

images and noted that the gas volume was significantly greater in cases with carmustine-loaded wafers than in cases with empty wafers.[7] Recently, Ohue et al. reported detailed serial changes in gas volume following Gliadel implantation and that gas appeared on the day after implantation in all patients, which increased until 1 week after surgery and disappeared within 3 months.[12]

The present study demonstrated more gas in the vicinity of the fixed carmustine wafer than in the vicinity of the fixed polyethylene disk at 24 h after placement. Therefore, it is difficult to explain the accumulation of gas around the carmustine wafer as representative of only trapped air between the wafer and fixing agents overlying it or gas production due to necrosis. The production of gas should be regarded as an intrinsic characteristic of the carmustine wafers placed into fluid. A previous study speculated that carbon dioxide may be produced at the breakdown of the matrix of the carmustine wafer considering the chemical structure.[12]

Limitations

There were a few limitations to this study. First, the experiment spanned 6 months, hence a portion of the placed objects in phantoms A and C became damaged at the last two time points of image acquisition. However, the influence of these damages was considered small because these damages were within the assumption range as described in **Materials and Methods**. Second, contamination of the signal from the surrounding materials as the result of a partial volume effect was reckoned inevitable on quantitative ROI analysis of the placed objects because of their extreme thinness (1.3 mm), even though great care was taken. Finally, the time interval after construction of the phantoms in this experiment did not accurately correspond to the time interval after surgery *in vivo*. *In vitro* phantoms cannot completely imitate the physiology of a surgical resection cavity, including its buffer capacity and substance carry-away rate. However, the serial changes observed in the present study can be regarded as a convincing example of the time course of the MRI and CT appearance of carmustine wafers without the effects from biological reactions.

Conclusion

Carmustine wafers *in vitro* showed serial imaging changes that reflect penetration of fluid inside the wafers and degradation of the hydrophobic matrix. The transient hyperintensity of carmustine wafers on T_1WIs observed in the clinical setting is considered attributable to the biological reactions to the wafers, whereas the initial production of gas is considered as an intrinsic characteristic of carmustine wafers.

Acknowledgments

This study was supported in part by the Grant-in-Aid for Scientific Research (C) (#26461830) from the Japan Society for the Promotion of Science.

Conflicts of Interest

The Gliadel wafers and the polyethylene disk used in this study were provided by Eisai Co., Ltd., Tokyo, Japan.

References

1. Lawson HC, Sampath P, Bohan E, et al. Interstitial chemotherapy for malignant gliomas: the Johns Hopkins experience. J Neurooncol 2007; 83:61–70.
2. Mangraviti A, Tyler B, Brem H. Interstitial chemotherapy for malignant glioma: future prospects in the era of multimodal therapy. Surg Neurol Int 2015; 6 (Suppl 1):S78–S84.
3. Leong KW, Brott BC, Langer R. Bioerodible polyanhydrides as drug-carrier matrices. I: characterization, degradation, and release characteristics. J Biomed Mater Res 1985; 19:941–955.
4. Fung LK, Ewend MG, Sills A, et al. Pharmacokinetics of interstitial delivery of carmustine, 4-hydroperoxycyclophosphamide, and paclitaxel from a biodegradable polymer implant in the monkey brain. Cancer Res 1998; 58: 672–684.
5. McGirt MJ, Than KD, Weingart JD, et al. Gliadel (BCNU) wafer plus concomitant temozolomide therapy after primary resection of glioblastoma multiforme. J Neurosurg 2009; 110:583–588.
6. Prager JM, Grenier Y, Cozzens JW, Chiowanich P, Gorey MT, Meyer JR. Serial CT and MR imaging of carmustine wafers. AJNR Am J Neuroradiol 2000; 21:119–123.
7. Hammoud DA, Belden CJ, Ho AC, et al. The surgical bed after BCNU polymer wafer placement for recurrent glioma: serial assessment on CT and MR imaging. AJR Am J Roentgenol 2003; 180:1469–1475.
8. Dyke JP, Sanelli PC, Voss HU, et al. Monitoring the effects of BCNU chemotherapy wafers (Gliadel) in glioblastoma multiforme with proton magnetic resonance spectroscopic imaging at 3.0 Tesla. J Neurooncol 2007; 82:103–110.
9. Della Puppa A, Rossetto M, Ciccarino P, et al. The first 3 months after BCNU wafers implantation in high-grade glioma patients: clinical and radiological considerations on a clinical series. Acta Neurochir (Wien) 2010; 152:1923–1931.
10. Colen RR, Zinn PO, Hazany S, et al. Magnetic resonance imaging appearance and changes on intracavitary Gliadel wafer placement: A pilot study. World J Radiol 2011; 3:266–272.
11. Ulmer S, Spalek K, Nabavi A, et al. Temporal changes in magnetic resonance imaging characteristics of Gliadel wafers and of the adjacent brain parenchyma. J Neurooncology 2012; 14:482–490.
12. Ohue S, Kohno S, Inoue A, et al. Evaluation of serial changes on computed tomography and magnetic resonance imaging after implantation of carmustine wafers in patients with malignant gliomas for differential diagnosis of tumor recurrence. J Neurooncol 2016; 126:119–126.
13. Masuda Y, Ishikawa E, Yamamoto T, et al. Early postoperative expansion of parenchymal high-intensity areas on T2-weighted imaging predicts delayed cerebral ede-

ma caused by carmustine wafer implantation in patients with high-grade glioma. Magn Reson Med Sci 2016; 15:299–307.
14. FDA's Docket Management - NDA # 20–637 GLIADEL® Wafer (Polifeprosan 20 with Carmustine Implant). https://www.fda.gov/ohrms/dockets/ac/01/briefing/3815b2_05_fda.pdf (Accessed Apr 23, 2017)
15. In den Kleef JJ, Cuppen JJ. RLSQ: T_1, T_2, and ρ calculations, combining ratios and least squares. Magn Reson Med 1987; 5:513–524.
16. Stanisz GJ, Odrobina EE, Pun J, et al. T_1, T_2 relaxation and magnetization transfer in tissue at 3T. Magn Reson Med 2005; 54:507–512.
17. Landis JR, Koch GG. The measurement of observer agreement for categorical data. Biometrics 1997; 33:159–174.
18. Brem H, Mahaley MS Jr, Vick NA, et al. Interstitial chemotherapy with drug polymer implants for the treatment of recurrent gliomas. J Neurosurg 1991; 74: 441–446.
19. Aoki T, Yamada S. II. [Current status of BCNU stent in the brain for treatment of glioma]. Gan To Kagaku Ryoho 2013; 40:708–717. (in Japanese)
20. Dang W, Daviau T, Brem H. Morphological characterization of polyanhydride biodegradable implant gliadel during *in vitro* and *in vivo* erosion using scanning electron microscopy. Pharm Res 1996; 13:683–691.
21. Brem H, Ewend MG, Piantadosi S, Greenhoot J, Burger PC, Sisti M. The safety of interstitial chemotherapy with BCNU-loaded polymer followed by radiation therapy in the treatment of newly diagnosed malignant gliomas: phase I trial. J Neurooncol 1995; 26:111–123.
22. Bjorenson JE, Grove HF, List MG Sr, Haasch GC, Austin BP. Effects of hemostatic agents on the pH of body fluids. J Endod 1986; 12:289–292.